Dynamics of Turing pattern monolayers close to onset

V. Dufiet and J. Boissonade
Centre de Recherche Paul Pascal, CNRS Bordeaux, Avenue Schweitzer, F-33600 Pessac, France
(Received 27 February 1995)

We perform simulations of Turing patterns confined to a monolayer by a gradient of parameters in a three-dimensional system. The results provide a more comprehensive basis for the interpretation of the actual experimental results than the usual, but disputable, interpretation in terms of ideal two-dimensional systems. Systematic comparison of the bifurcation behavior in genuine two-dimensional systems and in such monolayers is achieved with a theoretical model. We show that in the monolayers, hexagonal phases are restabilized as a result of the longitudinal instability. [S1063-651X(96)09905-9]

PACS number(s): 47.54.+r, 05.70.Ln, 82.20.Mj, 82.20.Wt

I. INTRODUCTION

Turing structures are self-organized stationary concentration patterns which result from the sole competition between reaction and diffusion in a class of chemical systems kept far from equilibrium by a permanent feed of fresh reactants. These chemical systems must exhibit the following features. First, the reaction kinetics is controlled by two antagonistic feedback loops, namely, an activation process—such as an autocatalytic reaction—and an inhibitory process. This set of properties is common to various types of ''active media'' that exhibit exotic temporal or spatial behavior, like multistability, periodic or chaotic oscillations, excitability, or wave propagation [1–5]. For Turing patterns to form, a species controlling the inhibitory process must diffuse much faster than any species controlling the activation process. First predicted in 1952 [6], they have been thoroughly investigated from a theoretical point of view (for reviews see Refs. [1, 4, 7]). Nevertheless, almost 40 years passed before they were experimentally evidenced with the so-called chlorite-iodine-malonic acid (CIMA) reaction [8], first in a gel strip reactor [9–11], then in a gel disk reactor [12,13]. The latter setup has become the most commonly used. It is made of a thin flat piece of gel with two opposite faces kept in contact with permanently refreshed reservoirs of different input solutions. The input species diffuse from the reservoirs into the gel where they meet and react. A gradient of the input reactants concentrations spontaneously develops in the direction orthogonal to the faces, establishing a continuous change of control parameters. A pattern, breaking the planar symmetry, will form in regions where the values of these local parameters meet the conditions for a Turing instability, i.e., in a thick stratum parallel to the faces (Fig. 1) [14]. In the actual experiments, the width of this stratum commonly reaches three or four wavelengths [15]. Thus—contrary to the well-known Rayleigh-Bérnard convective structures—they present a three-dimensional character. The patterns are normally looked at in a direction parallel to the gradient, so that the light absorption is averaged over the film thickness and there is some uncertainty on the true geometry of the structures. Nevertheless, when a control parameter is changed continuously, the width of the unstable region grows progressively. The structures are thus found to form one layer after the other, so that just beyond the pattern onset there is a single layer [16]. We shall call this type of pattern a ''monolayer.'' Transverse dimensions of reactors are large enough (more than 100 wavelengths) for the boundary effects to be negligible and these patterns are generally coherent and quite periodic over large size domains separated by topological defects. In these conditions, the most common regular planforms observed through the gel are stripes or hexagons. In regard of their quasi-two-dimensional character and the analogies in planforms, pattern selection theories developed for genuine two-dimensional (2D) system are commonly applied to the experimental monolayers.

Unfortunately, there is no definite evidence that the selection stability properties are identical in these genuine 2D patterns and in those restricted to a single layer bounded by a strong gradient of control parameters. There has been a number of analytical and numerical studies of patterns in a ramp of control parameters [11,17–27]. None of them really meet the requirements above. Analytical methods generally rely on slow parameter ramps in contradiction with such strong localization problems. Two-dimensional systems with parameter ramps may exhibit patterns made of a single row of dots, the 1D analog of the 2D monolayers [11,21], but this problem turns out to be of a different kind due to the nonexistence of rotational invariance in one dimension.

In order to clarify the relations between the genuine homogeneous 2D systems and the monolayers, we have studied the selection of patterns close to onset for the same model in both geometries. In Sec. II, we introduce a simple appropriate reaction-diffusion model that exhibits Turing patterns. Then we study the selection of patterns close to onset and check the numerical results with those predicted from a weakly nonlinear analysis. In Sec. III, we mimic a disk reactor by introducing a parameter ramp that induces the formation of monolayers in agreement with the experimental observations. On the basis of 3D numerical simulations we show that a transverse instability leading to the formation of a monolayer precedes a longitudinal instability. We show that, very close to onset, the monolayers behave like genuine 2D systems but that, in relation with the longitudinal instability, hexagonal phases are restabilized when the distance to threshold increases. This property is interpreted as a result of the coupling of the cubic terms with a homogeneous mode, in agreement with the recent theory of Price [28].

In the following, we call ''2D systems'' without further precision genuine two-dimensional systems with uniform control parameters. We always consider the relative stability

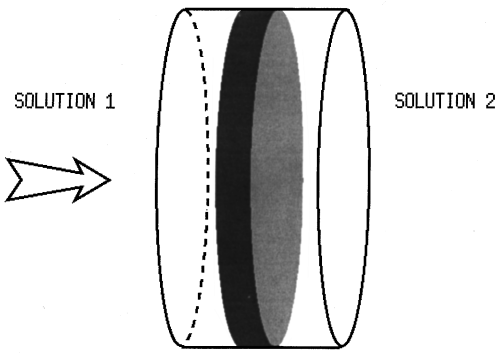

FIG. 1. Scheme of a disk reactor. Input reactants are provided by solutions 1 and 2. Structures form in the gray region. The arrow indicates the direction of observation.

of regular periodic patterns—stripes or hexagons patterns—without topological defects and assume periodic boundary conditions in the pattern plane. All 2D and 3D computations were performed with an implicit hopscotch method [29] tailored to handle the nonlinear terms [30].

II. TWO-DIMENSIONAL SYSTEMS

In order to make clear the comparison with the monolayers, we shall report rather extensively the analytical and numerical properties of the two-dimensional systems that will be used as a reference in Sec. III.

A. Reaction-diffusion model

The linearization around the stationary state of any two-variable reaction-diffusion system able to exhibit Turing patterns can always be written in the form

$$\frac{\partial u}{\partial t} = a_1 u - \eta a_2 v + D_u \nabla^2 u,$$

$$\frac{\partial v}{\partial t} = \eta a_3 u - a_4 v + D_v \nabla^2 v, \tag{1}$$

where $a_i > 0$, $\eta = \pm 1$, and D_u and D_v are the diffusion coefficients [4,31,32]. The model is called *activator-inhibitor* if $\eta = +1$ and *substrate-depleted* if $\eta = -1$. The number of coefficients can be reduced to three for each type of model by rescaling the concentrations, the time, and the space coordinates. Without lack of generality, we can restrict ourself to the activator-inhibitor type. Introducing the ratio $d = D_v/D_u$, a convenient form of the rescaled system is

$$\frac{\partial u}{\partial t} = u - \alpha v + \nabla^2 u,$$

$$\frac{\partial v}{\partial t} = u - \beta v + d\nabla^2 v, \tag{2}$$

with $\alpha > 0$ and $\beta > 0$. Variable u is the activator, whereas v is the inhibitor.

One can define a reaction-diffusion system that give rise to Turing patterns by adding a minimum of nonlinear terms to this set of equations:

$$\frac{\partial u}{\partial t} = u - \alpha v + \gamma u v - u^3 + \nabla^2 u,$$

$$\frac{\partial v}{\partial t} = u - \beta v + d\nabla^2 v. \tag{3}$$

The cubic term $-u^3$ limits the exponential growth of the perturbation and allows for the saturation of the instability. The quadratic term γuv avoids the invariance in the transformation $(u,v) \rightarrow (-u,-v)$, which is nongeneric in chemical systems. This particular symmetry can be restored by setting $\gamma = 0$. Although this model has not been derived from a chemical scheme, it exhibits the same properties and has been preferred in regard of its simplest analytical properties.

This model has a uniform stationary state $(u = v = 0)$ independent of the control parameters α, β, γ, d. The linear stability analysis of this stationary state—hereafter referred as the ''zero'' state—follows from the linearization of system (3) which actually reduces to Eqs. (2). In the absence of diffusion, the homogeneous system exhibits a Hopf bifurcation at $\beta = 1$ (when $\alpha > 1$) and an exchange of stability or a pitchfork bifurcation along the line $\alpha = \beta$. The stationary state is stable to any small homogeneous perturbation for $1 < \beta < \alpha$ (Fig. 2). When the diffusion terms are present, the stationary state can become unstable, in this parameter domain, to a nonuniform perturbation $\mathbf{u} = \mathbf{u_0} \exp(i\mathbf{k}\cdot\mathbf{r})$ of wave vector $\mathbf{k} \neq \mathbf{0}$, where $\mathbf{u} = \binom{u_1}{v_1}$. This Turing bifurcation occurs when the real part of an eigenvalue of the linear operator

$$L = \begin{pmatrix} 1 - k^2 & -\alpha \\ 1 & -\beta - dk^2 \end{pmatrix} \tag{4}$$

becomes positive, that is, when the determinant Δ and the first derivative $d\Delta/dk$ are simultaneously zero. The Turing bifurcation is located along the line AB (Fig. 2) defined by the equation

$$\alpha = \alpha_c = \frac{(\beta + d)^2}{4d}. \tag{5}$$

The critical wavenumber k_c is given by

$$k_c^2 = \frac{d - \beta}{2d}. \tag{6}$$

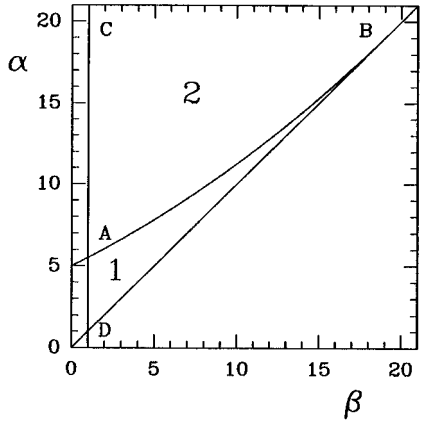

FIG. 2. Bifurcation diagram at $d = 20$. (1) Turing space. (2) Stable stationnaire state ($\beta > 1$). AB: limit of Turing bifurcation ($\beta < 20$). CD: limit of Hopf bifurcation ($\alpha > 1$).

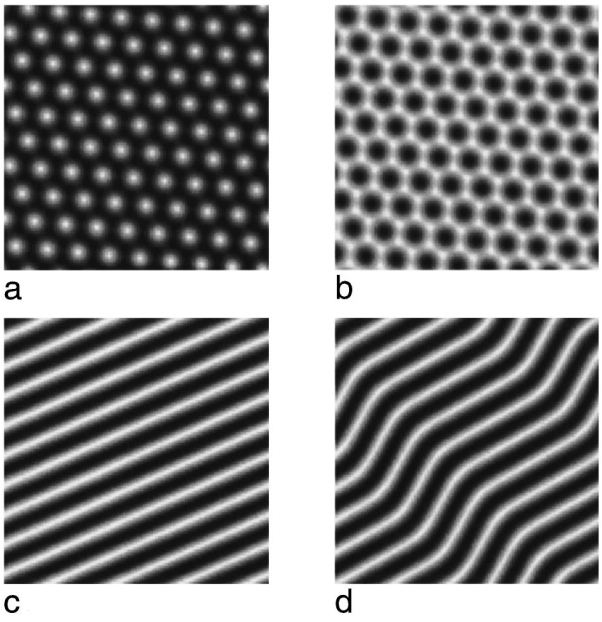

FIG. 3. Two-dimensional patterns. (a) hexagonal pattern H_0 ($\alpha=7.81$, $\beta=5$, $\gamma=0.75$, $d=20$, size: 100×100); (b) hexagonal pattern H_π ($\alpha=7.81$, $\beta=5$, $\gamma=0.75$, $d=20$, size: 100×100); (c) striped pattern ($\alpha=7.45$, $\beta=5$, $\gamma=1$, $d=20$, size: 100×100); (d) zigzag pattern ($\alpha=7.3$, $\beta=5$, $\gamma=1$, $d=20$, size: 100×100).

The parameter domain where the stationary state is unstable only to a nonuniform perturbation—sometimes called the ''Turing space'' [3]—is represented in Fig. 2. As expected, this domain exists only when the inhibitor species diffuses faster than the activator species and the area of this Turing space increases with the ratio d.

We shall now consider the formation and the selection of patterns close to the onset $\alpha=\alpha_c$—i.e., the line AB—and avoid as much as possible coupling with other instabilities, i.e., the vicinity of lines BD and CD.

If not otherwise stated, α is used as the expandable bifurcation parameter and the numerical simulations are carried out with the values $d=20$ and $\beta=5$. With this parameter set, the Turing bifurcation is located at $\alpha_c=7.8125$ and $k_c=0.6124$.

B. Weakly nonlinear theory and selection of patterns

Figure 3 illustrates the different types of stable stationary patterns that are found in numerical simulations when exploring the parameter space. The variable u is represented on a gray scale, changing from black (minimum value) to white (maximum value). The variable v changes in phase with u and exhibits similar patterns. When the patterns spontaneously emerge from a noisy initial unstable stationary state, they naturally contain topological defects that move and relax slowly. If the system is finite these defects tend to vanish on a long time scale. From now on, we shall consider only periodic patterns without topological defects. We also assume that they are stable to small charges of wavelength caused by cross-roll or phase instabilities [33].

All the patterns in Fig. 3 are made of stripes and hexagons. There are two types of hexagons, respectively referred to as H_0 and H_π, according to whether the minima or the maxima are disposed on the hexagonal lattice. Stripes can be straight lines or exhibit periodic undulations that result from a previous zigzag instability [34]. The latter still belong to the stripe pattern category. The planforms in Fig. 3 are identical to those observed with other chemical schemes, like the Schnackenberg model [35,36] or the Brussellator [37]. This supports the validity of this simplified model.

Close to onset, the eigenvalues associated to the critical modes are close to zero, so that they evolve on a long time scale, whereas the noncritical stable modes relax rapidly. The whole dynamics can be therefore reduced to the dynamics of the active slow modes, which slave the fast stable modes [2]. The stability and the selection of the different patterns close to onset can be derived from the amplitude equations that governs the dynamics of these active modes. Hexagonal and stripe patterns are thus well described by a system of three active resonant pairs of modes $(\mathbf{k}_i,-\mathbf{k}_i)_{i=1,2,3}$ making angles of $2\pi/3$.

Close to onset, the solutions are given by

$$\mathbf{u}=\mathbf{u}_0\cdot\sum_{\mathbf{k}_j}\left[A_j\exp(i\mathbf{k}_j\cdot\mathbf{r})+\mathbf{A}_j^*\exp(-i\mathbf{k}_j\cdot\mathbf{r})\right], \tag{7}$$

where $\mathbf{u}_0$ defines the direction of the eigenmodes in concentration space (i.e., the ratio u/v) and where A_j and the conjugate A_j^* are, respectively, the amplitude associated with modes $\mathbf{k}_j$ and $-\mathbf{k}_j$. From standard symmetry arguments, one can predict the general form of these amplitude equations at third order [38]:

$$\tau\frac{\partial A_1}{\partial t}=\mu A_1+\Gamma A_2^*A_3^*-[g|A_1|^2+g'(|A_2|^2+|A_3|^2)]A_1, \tag{8}$$

where $\mu=(\alpha_c-\alpha)/\alpha$ is a normalized distance to onset. Similar equations for A_2 and A_3 are obtained by circular permutation of indices. To avoid confusions, always keep in mind that, for model (3), the stationary state becomes Turing unstable when the bifurcation parameter α *decreases*, so that the distance to onset increases when the bifurcation parameter decreases.

The form of Eq. (8) is general for Turing bifurcations, but the exact expressions of the coefficients are specific to the model. Their derivation for our particular model (3) is reported in Ref. [30]. For amplitude of u, they are

$$\tau=\frac{2(d-1)}{\beta+d},\quad \Gamma=\frac{8d\gamma}{(\beta+d)^2}, \tag{9}$$

$$g=\frac{6d}{\beta+d}-\frac{16d^2\gamma^2(53\beta+23d)}{9(\beta-d)^2(\beta+d)^3}, \tag{10}$$

$$g'=\frac{12d}{\beta+d}-\frac{32d^2\gamma^2(3\beta+d)}{(\beta-d)^2(\beta+d)^3}.$$

For these amplitude equations to be valid, saturation of the instability must be achieved at third order. This condition is satisfied when

$$|\gamma|<\gamma_c=\frac{3\sqrt{3}(d^2-b^2)}{2\sqrt{2}[d(53\beta+23d]^{1/2}}. \tag{11}$$

For $\beta=5$ and $d=20$, $\gamma_c\approx5.721$, and the above conditions are satisfied for $|\gamma|=1$.

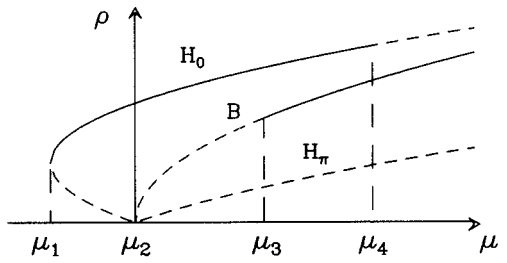

FIG. 4. Schematic bifurcation diagram for $\Gamma>0$. H_0: hexagonal patterns with $\Phi=0$; H_π: hexagonal patterns with $\Phi=\pi$; B: striped patterns; —: stable states, ---: unstable states. For $\Gamma<0$, the indices 0 and π must be exchanged.

Amplitudes in Eq. (8) can be written $A_j=\rho_j \exp \varphi_j$. It results from a standard stability analysis [26,38–40] that the only possible stable solutions are the steady state, a stripe pattern ($\rho_1\neq 0$, $\rho_2=\rho_3=0$) and the hexagonal patterns H_0 or H_π ($\rho_1=\rho_2=\rho_3$, with $\Phi=\varphi_1+\varphi_2+\varphi_3=0$ or π, respectively). Their existence and stability limits, as a function of the scaled bifurcation parameter μ, are ordered according to the scheme in Fig. 4 where the μ_i are given by

$$\mu_1=\frac{-\Gamma^2}{4(g+2g')}, \quad \mu_2=0,$$

$$\mu_3=\frac{\Gamma^2 g}{(g-g')^2}, \quad \mu_4=\frac{2g+g'}{(g'-g)^2}\,\Gamma^2. \tag{12}$$

Stable branches H_0 and H_π are mutually exclusive. The stable branch is H_0 if $\Gamma>0$ and H_π if $\Gamma<0$. A subcritical hexagonal branch comes out first at $\mu=\mu_1<0$ but loses stability when $\mu>\mu_4>0$. The supercritical stripe state branch is unstable close to the critical point but becomes stable for $\mu>\mu_3$. In the range $\mu_3<\mu<\mu_4$ both branches are stable. When $\gamma=0$ the nongeneric symmetry $(u,v)\rightarrow(-u,-v)$ is restored, one has $\Gamma=0$ and $\mu_1=\mu_2=\mu_3=\mu_4=0$. In this case, the stripe pattern bifurcates supercritically whereas the stability range of the hexagonal pattern vanishes. The latter is indeed directly related to the quadratic term Γ and proportional to γ^2 [41], in the model $\Gamma\propto\gamma$ so this stability range can be easily tuned.

The amplitude and stability of patterns obtained by direct numerical simulations and those obtained from the Eq. (8) are reported in Fig. 5 for $\gamma=0$ and $\gamma=0.75$ as a function of the distance to onset $\alpha_c-\alpha$. Close to onset, these results are in excellent agreement and confirm the validity of the approach.

When the nonlinear coefficients of the model also depend on the bifurcation parameter, the coefficients in Eq. (8) and the μ_i's may also depend on μ so that *one* of the hexagonal phases can regain stability at large μ. This direct reentrant phenomenon depends on the model and has been extensively discussed for the Brussellator [37] and for the Schnackenberg model [30,36]. Our model (3) avoids such a behavior that could bias the interpretation of results in Sec. III. However, Price has recently shown that hexagonal phases can be also restabilized—even in the absence of quadratic terms—if an active *homogeneous* mode, commonly referred as a d.c. mode, is present [28]. This can be found in particular when an homogeneous bifurcation occurs at some distance beyond

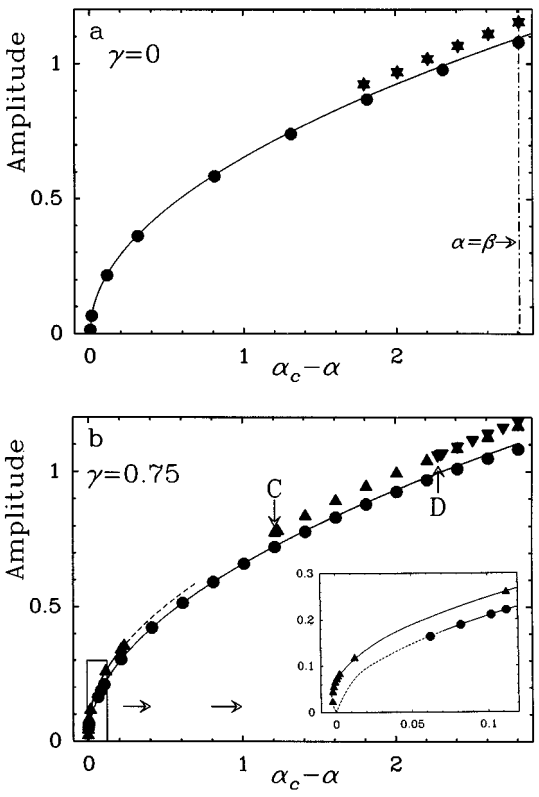

FIG. 5. Bifurcation diagrams of 2D system for model defined by Eqs. (3). ●: stable stripes, ▲: stable hexagons, H_0 (limit at C), ▼: stable hexagons H_π, (limit at D) (numerical simulation), —: stable states, ---: unstable states [computed from amplitude equations (8)–(10)]. (a) $\beta=5$, $\gamma=0$, $d=20$. (b) $\beta=5$, $\gamma=0.75$, $d=20$.

onset, as in our model at $\alpha=\beta$. In the vicinity of such bifurcations, the homogeneous mode becomes active and has to be included in the amplitude equations. Cubic interaction involving such an active mode of zero wave vector $\mathbf{0}$ generates in Eq. (8) a term of the form $A_0A_1^*A_2^*$. This term originates in the conservation law $\mathbf{k}_1=-\mathbf{k}_2-\mathbf{k}_3+\mathbf{0}$, where $(\mathbf{k}_1,\mathbf{k}_2,\mathbf{k}_3)$ is the basic triplet of the hexagonal structure. As it contains $A_2^*A_3^*$ like the quadratic term in Eq. (8), it plays the same stabilizing role for the hexagonal patterns. Nevertheless, if no other quadratic terms are present, H_0 and H_π are equivalent and are *both* restabilized. If there are quadratic terms in the dynamical equations [$\gamma\neq 0$ for model (3)], one of these pattern is favored and is restabilized first. This restabilization is shown in Fig. 5 for model (3) when α comes close to β. As expected, H_0 and H_π are both reentrant, at a common value $\alpha=\alpha_{R2}=6.02$ (i.e., $\alpha_c-\alpha_{R2}=1.7925$) for $\gamma=0$ [Fig. 5(a)], at different values for for $\gamma\neq 0$ [Fig. 5(b)]. In any case, the bifurcation scheme in Fig. 4 is preserved, provided that γ remains small enough. Note that since the wave vector of the faster growing mode gradually change with the distance to onset, the reentrant branches are actually only (re)stabilized for wave vectors slightly different of k_c. Those represented in Fig. 5 correspond to the wavevectors at which this restabilization occurs at the closest point to onset (respectively, $k_c\approx 0.55$ at $\gamma=0$ and $k_c\approx 0.57$ at $\gamma=0.75$). We shall see in Sec. III that the restabilization of hexagonal planforms by a d.c. mode can derive in a more indirect way from a different type of bifurcation.

III. MONOLAYERS

A. Monolayer modeling

We shall mimic the behavior of the experimental three dimensional disk reactors by introducing permanent gradients of at least one of the bifurcation parameters. In real disk reactors the input species concentrations are actually kept constant only on the feed surfaces but their gradients inside the gel are controlled both by diffusion and reaction. Thus, there is a feedback on the control parameters so that they are dynamical variables of the problem. Although such feedbacks can be incorporated in theoretical calculations [21], they depend on the specific form of the model. Nevertheless, in many cases, the reaction dynamics can be described by reduced models in which the control parameters are not the concentrations of input species themselves, but are effective constants, obtained by adiabatic eliminations or approximations on numerous variables. The experimental control parameters enter the equations through these constants. For instance, some of these species can be precursors that produce intermediate species at rates depending mainly on the input concentrations (a formal example is the Schnackenberg model [11]). Close to onset, supercritical Turing structures correspond to small amplitude spatial oscillations around the unstable stationary state. These small modulations are generally smoothed out and averaged in the feedback. In practice, one can thus assume that the spatial profiles of the control parameters are not coupled to these small variations of concentrations. For example, Lengyel and Epstein have proposed a satisfactory model of the ($ClO_2^{\cdot}$-I^--malonic acid) reaction, a variant of the CIMA reaction which is also known to give Turing patterns [42]. They have shown that the whole set of reactions can be approximated by a two-variable model in a large range of parameters. The control parameters only depend on the feed concentrations and on the distance to the feed surfaces. They can be tuned independently in order that the system become supercritical in a layer parallel to the faces [14], i.e., the conditions expected to produce monolayers. Although the extension of these conclusions to the CIMA reaction or other models is not straightforward, modeling monolayers by introducing a tunable parameter profile appears to be a sound approach. The exact form of the model and of this profile do not seem critical for the conclusions that we shall draw in Sec. IV, provided that a few prerequisites accounting for experimental conditions are met.

In agreement with Sec. I, the following requirements must be retained: (a) The control parameter in the reaction-diffusion equations, say, α in Eq. (3), must change continuously along the sole direction $\mathbf{O_z}$, orthogonal to the opposite faces, and remain uniform in directions $\mathbf{O_x}$ and $\mathbf{O_y}$, parallel to these faces. (b) The profile of this primary parameter must be controlled through one (or several) tunable secondary control parameters that play the role of the tunable experimental constraints. (c) The primary control parameter must be subcritical on the faces (at $z=0$ and $z=L$) and take supercritical values over a range ΔL located at some distance from these faces. In the explored range of tunable parameters, ΔL must grow from zero to $\Delta L \sim \lambda$, in order to go from a uniform state to a structure extending over at least one wavelength along the direction $\mathbf{O_z}$. When ΔL further grows, multilayer structures settle. Such structures are beyond the scope of this paper.

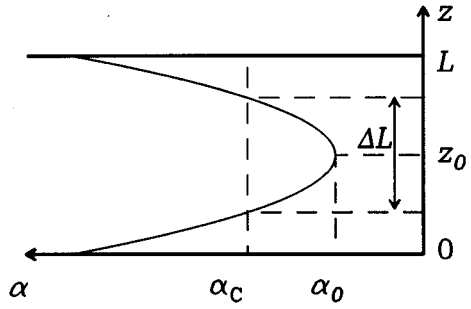

FIG. 6. Control parameter profile.

So far, there is no conclusive experimental argument to chose a particular parameter profile meeting these conditions. Thus we have retained a simple form, that is, a parabolic profile centered on the median plane $z=\frac{1}{2}L$. *A priori*, this gradient could be applied to any coefficient of the linearized equations. Since the different coefficients of the linearized equations [before scaling in order to keep all of them; see Eq. (1)] play different roles in the dynamics, one could expect that the properties depend of the choice of the coefficient on which the gradient is applied. Whichever coefficient is concerned, the results actually happen to be similar. This point will be briefly checked at the end of this section. The results extensively reported in this section have been obtained with the model (3) with the following spatial control parameter profile:

$$\alpha(z)=\alpha_0+\rho(z-z_0)^2. \tag{13}$$

Parameter ρ was kept fixed in each series of numerical experiments whereas α_0 was used as the tunable parameter. The function $\alpha(z)$ is maximum in the median plane $z=z_0=L/2$, where $\alpha(z)=\alpha_0$—the most supercritical value—and define a supercritical domain ΔL, where $\alpha(z)<\alpha_c$ centered on this median plane (Fig. 6). When comparing bifurcation diagrams of the 2D uniform systems of Sec. II with those of these 3D gradient systems, it is natural to use respectively α and α_0, or the distances to onset $\Delta\alpha=\alpha_c-\alpha$ and $\Delta\alpha_0=\alpha_{c0}-\alpha_0$.

Since the zero stationary state of our particular model is independent of the primary parameter α, the spatial organization results unambiguously from the Turing instability and cannot be confused with trivial spatial changes of the stationary state.

Two types of instabilities may occur according to the orientation of the wave vector.

A longitudinal instability, if the critical wave vector noted $\mathbf{k}_\parallel$, is oriented parallel to the gradient (orthogonal to the faces). The critical parameter can be determined in a 1D system colinear to the parameter gradient since, in this case, it is the only possible instability.

A transverse instability, if the critical wave vector noted $\mathbf{k}_\perp$, is oriented orthogonal to the gradient (parallel to the faces). This transverse mode is rotationally invariant in planes parallel to the faces. When a monolayer is considered as a 2D system, the wave vector $\mathbf{k}_\perp$ matches with $\mathbf{k}$.

Section III B is devoted to the determination of the first linear instability leading to a Turing structure and the form

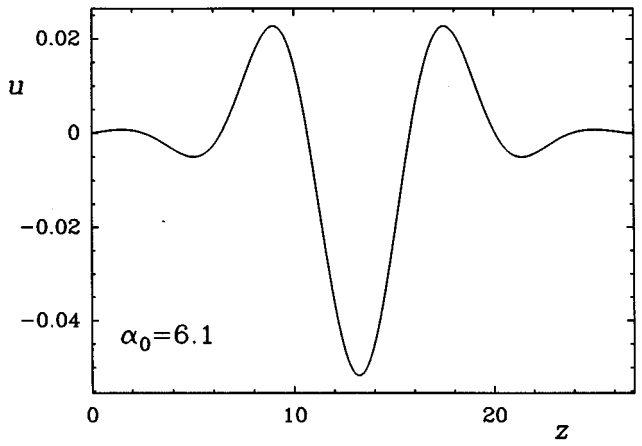

FIG. 7. Concentration profile $u(z)$ in the 1D system. $\alpha_0=6.1$, $\rho=0.15$, $\beta=5$, $\gamma=1$, $d=20$.

of the dispersion curve in the 3D systems described above. In Sec. III C, we report the bifurcation diagrams close to onset and the relative stability of the different patterns. These numerical results are compared to those obtained in Sec. II for genuine 2D systems and we discuss the limits of the concept of ''monolayer.'' From now on, fixed parameters are given the following values: $\beta=5$, $d=20$, $\rho=0.15$. The linear properties are independent of the parameter γ, which is involved only in nonlinear terms.

B. Linear instability

We have determined the onset of the longitudinal instability by numerical simulation of a 1D system. The uniform stationary state becomes unstable for $\alpha_0>\alpha_{\|}\simeq 6.16$. The inhomogeneous profile just beyond the transition is given in Fig. 7. The transition does not occur for $\alpha_0=\alpha_c=7.8125$, but is delayed until the width of the supercritical domain is larger than a critical value, here when $\Delta L\approx 0.65\lambda$.

The transverse instability was studied by following the emergence of a pattern in the median plane. We have determined, not only the onset of this instability, but also the dispersion curves $\sigma(\mathbf{k}_\perp)$ (Fig. 8) by following, after the fast relaxation onto the unstable eigenvector, the growth of a small perturbation of wavevector $\mathbf{k}_\perp$ and amplitude A. Since, in the linear regime, the amplitude grows according to the

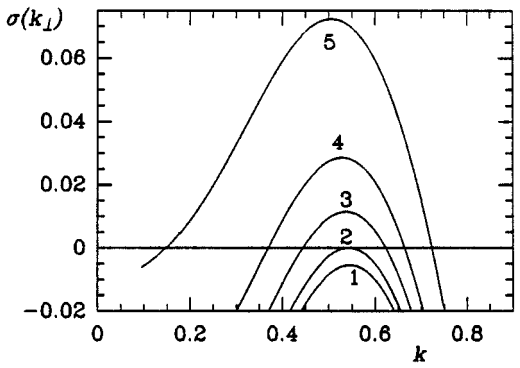

FIG. 8. Dispersion curves: growth rate $\sigma(k_\perp)$ for different α_0 values. (1) $\alpha_0=7.2$, (2) $\alpha_0=7.1350$, (3) $\alpha_0=7$, (4) $\alpha_0=6.8$, (5) $\alpha_0=6.3$.

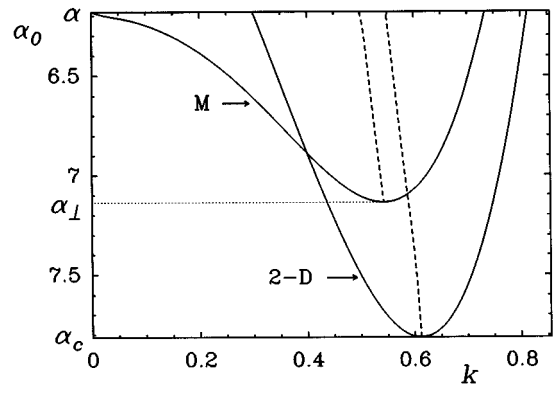

FIG. 9. Marginal stability curves of 2D and monolayer (M) systems. $\sigma(k_\perp)$ is maximal on dotted lines.

equation $dA/dt=\sigma(k_\perp)A$, where $k_\perp=|\mathbf{k}_\perp|$, the eigenvalue σ is constant in time and given by

$$\sigma(k_\perp)=\frac{\ln\left(\dfrac{A(t+\Delta t)}{A(t)}\right)}{\Delta t}. \tag{14}$$

A comparison of the upper and the lower limits of the unstable band as a function of α_0 with those obtained analytically for the genuine 2D systems is given in Fig. 9. The transverse instability is delayed to $\alpha_0=\alpha_\perp\simeq 7.135>\alpha_c$, i.e., $\Delta L\approx 0.41\lambda$. However, since $\alpha_\perp>\alpha_{\|}$, this transverse instability precedes the longitudinal instability, so that the critical value is $\alpha_{0c}=\alpha_\perp$ and $\Delta\alpha_0=\alpha_\perp-\alpha_0$.

A significant feature of the monolayer system is that the sideband rapidly expands on the lower side of $k_\perp$ when the distance $\Delta\alpha_0$ increases. The transverse mode $k_\perp=0$ becomes actually unstable for $\alpha_0=\alpha_{\|}$. Therefore, the longitudinal instability behaves like an homogeneous instability for the structures that develop in the transverse direction. This property will take a major importance in the interpretation of the nonlinear properties in Sec. III C. Another noticeable difference with the genuine 2D case is the shift to lower values of the wave vector corresponding to the maximum growth, i.e., the most unstable mode.

In order to check that the succession of the instabilities does not depend on the choice of the linear coefficient on which the parameter ramp is applied, we have successively applied this ramp to the coefficients α,β or to the coefficients α' and β' which come from a different normalization of the linearised equations:

$$\begin{aligned}\frac{\partial u}{\partial t}&=\alpha' u-v,\\ \frac{\partial v}{\partial t}&=\beta' u-v.\end{aligned} \tag{15}$$

We have kept the parabolic profile but the factor ρ has been adjusted to meet the conditions that define a monolayer system, but, to avoid additional spurious effects, we have required that for the most subcritical values the system do not comes close to an unstationary instability [e.g., when $\beta(z)\sim 0$]. In this purpose the parabolic profile is limited to the central region and limited to a nondangerous constant subcritical value elsewhere (e.g., $\beta=1.5$). These minor

TABLE I. Values of computed critical parameters.

Model	Control parameters	ρ	2D system	Transverse instability (ΔL)	Longitudinal instability (ΔL)
$\begin{pmatrix} 1 & -\alpha \\ 1 & -\beta \end{pmatrix}$	$\beta=5$	0.15	$\alpha_c=7.8125$	$\alpha_\perp=7.135$ (0.41λ)	$\alpha_\parallel=6.16$ (0.65λ)
$\begin{pmatrix} 1 & -\alpha \\ 1 & -\beta \end{pmatrix}$	$\alpha=7$ $\beta\geqslant 1.4$	−0.15	$\beta_c=3.66$	$\beta_\perp=4.53$ (0.49λ)	$\beta_\parallel=5.77$ (0.76λ)
$\begin{pmatrix} \alpha' & -1 \\ \beta' & -1 \end{pmatrix}$	$\beta'=2$ $\alpha'>0$	−0.012	$\alpha'_c=0.582$	$\alpha'_\perp=0.640$ (0.36λ)	$\alpha'_\parallel=0.783$ (0.67λ)
$\begin{pmatrix} \alpha' & -1 \\ \beta' & -1 \end{pmatrix}$	$\alpha'=0.6$	0.1	$\beta'_c=2.112$	$\beta'_\perp=1.599$ (0.37λ)	$\beta'_\parallel=1.067$ (0.53λ)

changes are always located well outside the core of the monolayer [43] The values of the computed critical parameter are collected in Table I.

Whichever the ramped coefficient is, both instabilities are always delayed and the transverse instability always comes first. This precedence was also predicted some time ago by Dewel *et al.* [20], on the basis of slightly different hypotheses. We shall now focus exclusively on model (3) in the case where the spatial profile is set on parameter α.

C. Stability and pattern selection

To analyze the two-dimensional symmetries of the different monolayer patterns, one can use different concentration amplitudes. Natural choices are the concentrations in the median plane, that is the most supercritical region with the higher contrast, or the spatial average of concentrations over the system depth, i.e., over the range $0<z<L$. The latter representation more closely mimics the experimental observation in the disk reactor. In practice, there is no qualitative differences between these two descriptions, as shown in Fig. 10, where both representations of the same monolayer of hexagonal symmetry are given. To evidence the monolayer character of the structure, a vertical section parallel to $\mathbf{O_x}$ is also shown. Other plane sections parallel to the faces exhibit the same symmetry, so that one can refer to the 2D terminology to classify the monolayers. If not otherwise stated, the reported amplitudes will always correspond to the concentrations in the median plane.

In Fig. 11, the different kinds of monolayer patterns observed in our numerical simulations are collected. They exhibit precisely the same planforms as the genuine 2D systems, that is hexagons H_0 or H_π, and straight or zigzag stripes (compare with Fig. 3).

The bifurcation diagrams for the monolayers at $\gamma=0.75$ are reported in Fig. 12. The wavelength is set to the critical value. Note that, contrary to diagrams of Sec. II, full and dotted lines do not represent analytical predictions, but are

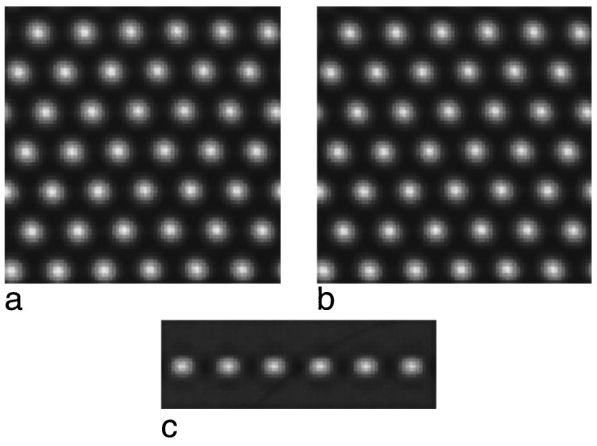

FIG. 10. Monolayer pattern. $\alpha_0=7$, $\rho=0.15$, $\beta=3$, $\gamma=3$, $d=20$, size: 80×80×27. (a) distribution of concentration u in the median plane; (b) distribution of concentration u averaged over the system depth; (c) distribution of concentration u in a plane ($\mathbf{O}_x$,$\mathbf{O}_z$) parallel to the parameter gradient.

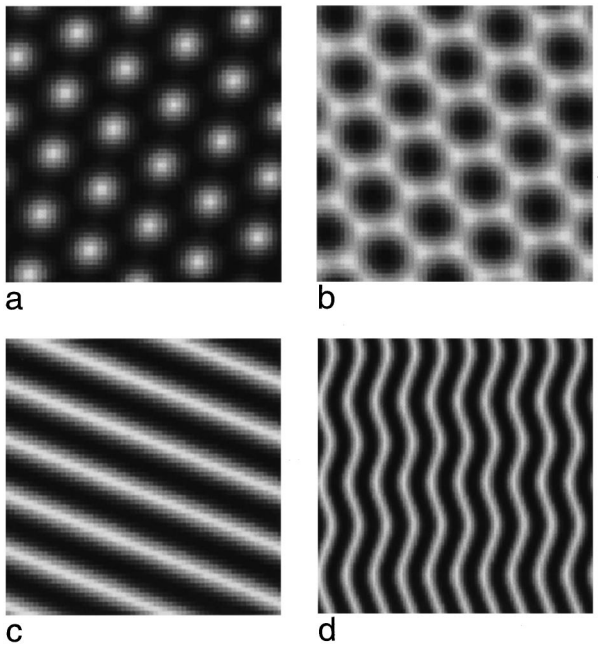

FIG. 11. Monolayer patterns: distribution of concentration u in the median plane. Common parameters: $\rho=0.15$, $\beta=5$, $d=20$. (a) hexagonal pattern H_0 ($\alpha_0=7$, $\gamma=3$, size: 60×60×27); (b) hexagonal pattern H_π ($\alpha_0=7$, $\gamma=-3$, size: 60×60×27); (c) striped pattern ($\alpha_0=7$, $\gamma=0$, size: 60×60×27); (d) zigzag pattern ($\alpha_0=6.6$, $\gamma=3$, size: 127×127×27).

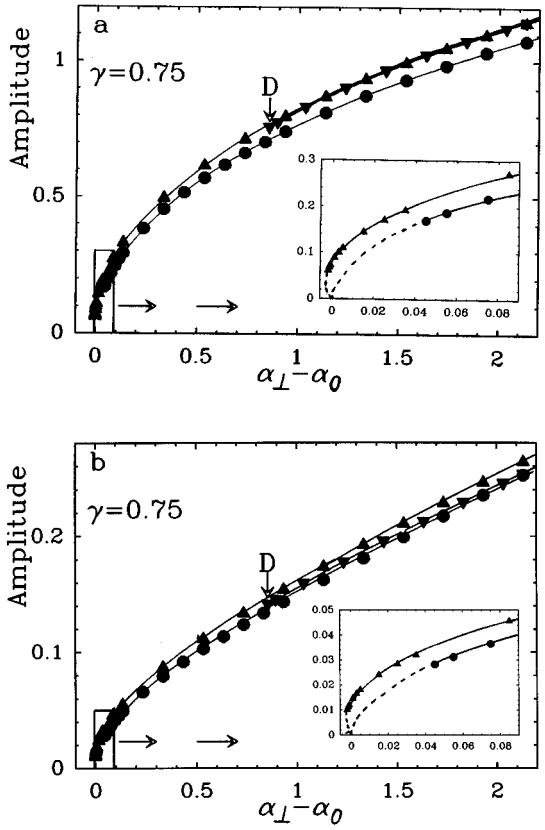

FIG. 12. Bifurcation diagrams for monolayers at $\gamma=0.75$ (amplitude of variable u). $\rho=0.15$, $\beta=5$, $d=20$. ▲: stable hexagons H_0. ▼: stable hexagons H_π (limit at point D). ●: stable stripes. —: stable states. ---: unstable states (numerical simulation). (a) amplitude in the median plane, (b) amplitude averaged over the system depth.

drawn to highlight the continuity of the numerical branches. In Fig. 12(a), we used the amplitude $A_{\max}$ in median plane, whereas in Fig. 12(b), we used the amplitude A_{ave} averaged over the system depth. As expected, both diagrams exhibit the same qualitative behavior. Close to onset, they are similar to those of 2D systems. The hexagonal form H_0 bifurcates first in a subcritical way. The stripe pattern branch is supercritical but is unstable nearly beyond onset. It recovers stability at some distance from the bifurcation point.

Close to onset, the amplitude A_{ave} remains finite. This attests that the layer thickness δ does not vanish at the critical point. This thickness can actually been estimated from the values of the maximum and averaged amplitude if one assume that the amplitude of a fully developed structure averaged on a wavelength should be about $A_{\max}/2$. In our system, one has $L/\lambda\sim 3$. From Figs. 12(a) and 12(b) one gets $A_{\max}/A_{\text{ave}}\sim 6\sim 2L/\lambda$ from which we can give an estimated value $\delta\sim 2LA_{\text{ave}}/A_{\max}\sim\lambda$. Therefore, at onset, the layer arises at once with a thickness of one wavelength. When $\gamma\neq 0$, this in agreement with the subcritical character of the bifurcation but in contrast with the analog problem in lower dimensions. Actually, in two-dimensional systems where one imposes a gradient of input reactant concentrations, the transition was essentially found to be supercritical [21].

Although, in the close vicinity of the bifurcation point, genuine 2D systems and monolayers exhibit similar stability

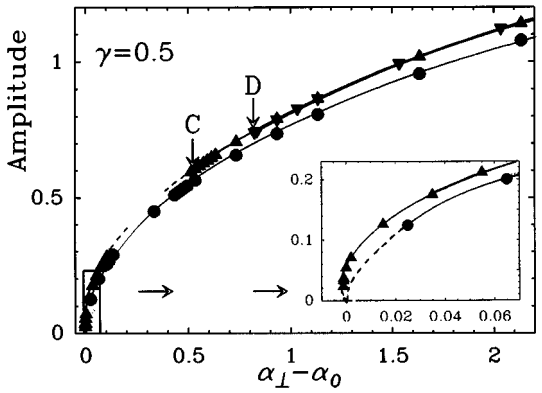

FIG. 13. Bifurcation diagram for the monolayers at $\gamma=0.5$ (amplitude of variable u). $\rho=0.15$, $\beta=5$, $d=20$. ▲: stable hexagons H_0 (limit at point C). ▼: stable hexagons H_π (limit at point D). ●: stable stripes. —: stable states. ---: unstable states (numerical simulation).

properties, in the latter, the hexagonal phase H_0 does not lose stability away from onset. For smaller values of γ, the hexagonal branch loses indeed its stability (see Fig. 13, $\gamma=0.5$), vanishing as expected when $\gamma=0$ (Fig. 14), but retrieves rapidly this stability at larger values of $\Delta\alpha_0$ as shown in Figs. 13 and 14. Whichever the value of γ is, a stable branch of H_π hexagons also comes out at some distance from onset. Contrary to the two dimensional case of Figs. 5, this branch exists at $k=k_c$. When $\gamma=0$, the stability ranges of the branches H_0 and H_π merge. In Fig. 15, we represent the different stability domains as a function both of $\Delta\alpha_0=(\alpha_\perp-\alpha_0)$—the distance to onset—and of the parameter γ. The stability limits are identical for γ and $-\gamma$ except that the hexagon types H_0 and H_π are exchanged.

IV. DISCUSSION AND CONCLUSION

We have shown that close to onset, 2D systems and monolayers have similar stability properties but that in the latter, when the distance to onset increases, both hexagonal phases are strongly restabilised. In the range where stripe patterns are also stable, patterns that form spontaneously from random fluctuations of the uniform state are indeed

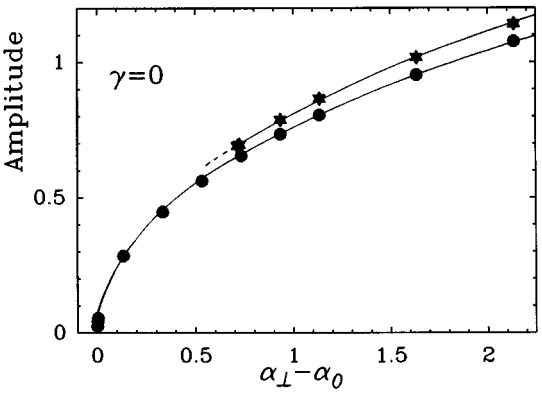

FIG. 14. Bifurcation diagrams for the monolayers at $\gamma=0$, $\rho=0.15$, $\beta=5$, $d=20$. ▲: stable hexagons H_0 and H_π. ●: stable stripes. —: stable states. ---: unstable states (numerical simulation).

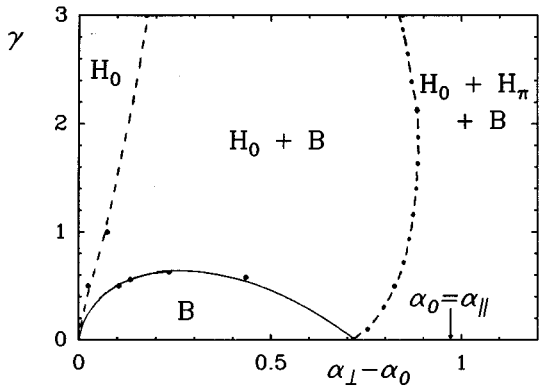

FIG. 15. Nature and stability of patterns in the parameter space (α_0,γ). $\rho=0.15$, $\beta=5$, $d=20$. —: stability limit of hexagons H_0. -·-·-: stability limit of hexagons H_π. ---: stability limit of stripes. H_0, H_π, and B, respectively, specify the stability region of patterns H_0, H_π, and stripes.

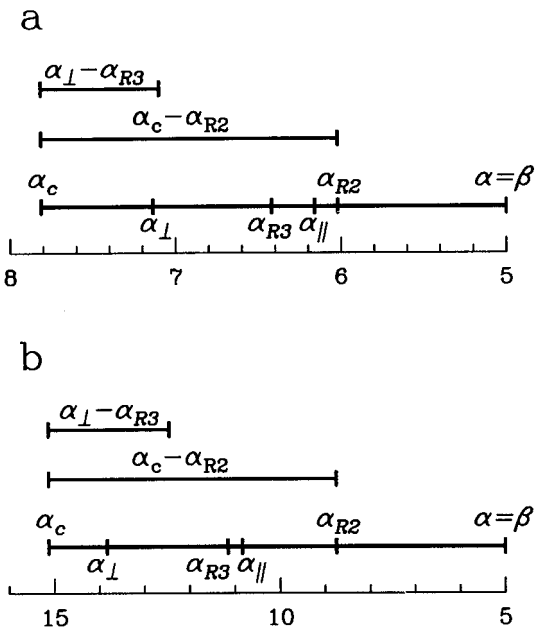

FIG. 16. Summary of relevant stability limits in 2D and monolayer systems. All quantities are defined in the text. (a) $\gamma=0$, $\beta=5$, $d=20$, $\rho=0.15$; (b) $\gamma=0$, $\beta=5$, $d=50$, $\rho=0.25$.

stripes, but this does not dismiss the importance of these hexagonal phases. Since the latter usually bifurcate first, they can be maintained afterwards by a slow continuous change of tunable parameters such as α_0 or γ. This should be a widespread situation in real experiments, where the concentrations gradients build up progressively from the initial state without physical break off. Simultaneous stabilization and/or reentrance of *both* types of hexagonal patterns suggests a d.c. mode induced reentrance. Although we have shown in Sec. II B, that the 2D model exhibits such a phenomenon in relation with a transcritical or pitchfork bifurcation at $\alpha=\beta$, this reentrance has a different origin in the monolayers. Due to the delayed bifurcation, it is more pertinent to use the deviations to onset $\Delta\alpha$ and $\Delta\alpha_0$ than the parameters α and α_0 to compare the stability of the 2D systems and of the monolayers. Accordingly, the restabilization of hexagonal phases turns out to be strongly advanced in the monolayers, as illustrated in Fig. 16(a) in the case $\gamma=0$. This particular example was chosen for simplicity since there is no hexagonal pattern at onset and since H_0 and H_π are both reentrant at the same value $\alpha=\alpha_{R3}$. The shift suggests that the origin of the d.c. mode is different in the two types of systems. Moreover, α_{R3} is close to $\alpha_\parallel$, the value at which the longitudinal instability occurs. To corroborate this point, the numerical simulations have been repeated with $d=50$ [Fig. 16(b)]. In the monolayers the restabilization point is again significantly advanced, but remains still located nearby the longitudinal instability. As we have shown in Sec. II B, this instability actually behaves like a homogeneous instability (d.c. mode) for the transverse structures of wave vector $k_\perp$. It is thus natural that the coupling with this mode restabilizes these transverse hexagonal structures that constitute the monolayer, in agreement with the Price theory. Therefore, the origin of the d.c. mode is quite different in the genuine 2D systems and in the monolayers. In the former, it resulted from the specific form of the reactive part (and could be absent in other models), whereas, in the latter, it follows from the ''geometric'' effect induced by the concentrations gradients that confine the structure. It is an intrinsic property of these monolayers.

So far, we have used a control parameter profile symmetric with respect to the plane $z=\frac{1}{2}L$. However, we have checked that the properties reported above do not depend on this particular choice by replacing the symmetric parabola by two half-parabolas with different curvatures [30]. The results are definitely similar to those of Sec. III and are not reported here.

In conclusion, we have shown than monolayer Turing patterns arise from a transverse instability with a delay when compared to the genuine 2D systems. The first pattern develops over a full wavelength in the direction $\mathbf{O_z}$. Very close to onset, monolayers and 2D patterns exhibit similar stability properties, but important changes occur in the vicinity of the longitudinal instability: the dispersion curve stretches toward a d.c. mode and, consequently, both hexagonal patterns H_0 and H_π are (re)stabilized. Thus, one can say that the patterns lose their two-dimensional character close to this longitudinal instability. Nevertheless, this instability does not correspond to any visual qualitative change of the structure—visible multiple layers actually come far beyond the transition—so that it seems experimentally impossible to distinguish the narrow parameter range where the 2D description is valid from that of the ambiguous—between 2D and 3D—regime that comes next. Thus, contrary to what is commonly accepted, one should be very cautious in the application of the well developed 2D pattern selection formalism to the experimental results, even when the structure is restricted to a single layer.

ACKNOWLEDGMENTS

We greatly acknowledge P. De Kepper for a critical reading of the manuscript and E. Dulos, P. Borckmans, G. Dewel, A. De Wit, and C. Price for numerous fruitful discussions. This work has been supported by the European Community Science program (Contract No. SC1-CT91-0706).

[1] G. Nicolis and I. Prigogine, *Self-organization in Nonequilibrium Chemical Systems* (Wiley, New York, 1977).
[2] H. Haken, *Synergetics, an Introduction* (Springer-Verlag, Berlin, 1977).
[3] R. J. Field and M. Burger, *Oscillations and Traveling Waves in Chemical Systems* (Wiley, New York, 1985).
[4] J. D. Murray, *Mathematical Biology* (Springer-Verlag, Berlin, 1989).
[5] A. S. Mikhailov, *Foundations of Synergetics I* (Springer-Verlag, Berlin, 1990); A. S. Mikhailov and A. Y. Loskutov, *Foundations of Synergetics II* (Springer-Verlag, Berlin, 1991).
[6] A. M. Turing, Philos. Trans. R. Soc. London B **327**, 37 (1952).
[7] R. Kapral and K. Showalter, *Chemical Patterns and Waves* (Kluwer, Amsterdam, 1995). This reference contains several feature articles on Turing patterns.
[8] P. De Kepper, J. Boissonade, and I. Epstein, J. Phys. Chem. **94**, 6525 (1990).
[9] V. Castets, E. Dulos, J. Boissonade, and P. De Kepper, Phys. Rev. Lett. **64**, 2953 (1990).
[10] P. De Kepper, V. Castets, E. Dulos, and J. Boissonade, Physica D **49**, 161 (1991).
[11] J. Boissonade, in *Bifurcation and Chaos: Analysis, Algorithms, Applications*, edited by R. Seydel, F. W. Schneider, T. Küpper, and H. Troger, Int. Ser. Num. Math. Vol. 97 (Birkhäuser, Basel, 1991), p. 67.
[12] Q. Ouyang and H. L. Swinney, Nature **352**, 610 (1991).
[13] Q. Ouyang and H. L. Swinney, Chaos **1**, 411 (1991).
[14] I. Lengyel, S. Kádár, and I. Epstein, Phys. Rev. Lett. **69**, 2729 (1992).
[15] Q. Ouyang, Z. Noszticzius, and H. L. Swinney, J. Phys. Chem. **96**, 6773 (1992).
[16] J. Boissonade, E. Dulos, and P. De Kepper, in *Chemical Patterns and Waves* (Ref. [7]), p. 221.
[17] M. Herschkowitz-Kaufman and G. Nicolis, J. Chem. Phys. **56**, 1890 (1972).
[18] J. F. Auchmuty and G. Nicolis, Bull. Math. Biol. **37**, 323 (1975).
[19] L. Kramer, E. Ben-Jacob, H. Brand, and M. C. Cross, Phys. Rev. Lett. **49**, 1891 (1982).
[20] G. Dewel, D. Walgraef, and P. Borckmans, J. Chim. Phys. (France) **84**, 1335 (1987).
[21] J. Boissonade, J. Phys. (France) **49**, 541 (1988).
[22] G. Dewel and P. Borckmans, Phys. Lett. **138**, 189 (1989).
[23] A. De Wit, P. Borckmans, and G. Dewel, in *Instabilities and Nonequilibrium Structures IV*, edited by E. Tirapegui and W Zeller (Kluwer, Amsterdam, 1993).
[24] B. A. Malomed and A. A. Nepomnyaschy, Europhys. Lett. **21**, 195 (1993).
[25] B. A. Malomed, Phys. Rev. E **47**, R2257 (1993).
[26] P. Borckmans, G. Dewel, A. De Wit, and D. Walgraef, in *Chemical Patterns and Waves* (Ref. [7]).
[27] A. De Wit, Ph.D. Thesis, U.L.B., Brussels, 1994.
[28] C. Price, Phys. Lett. A **194**, 385 (1994); G. Dewel, S. Metens, M'F. Hilali, P. Borckmans, and C. B. Price, Phys. Rev. Lett. **74**, 4647 (1995).
[29] A. R. Gourlay, J. Inst. Math. Appl. **6**, 375 (1970); A. R. Gourlay and G. R. McGuire, *ibid*. **7**, 216 (1971).
[30] V. Dufiet, Ph.D. Thesis, Univ. of Bordeaux, 1994.
[31] H. Fujii H., M. Mimura, and Y. Nishiura, Physica D **5**, 1 (1982).
[32] A. Hunding, Physica A **188**, 172 (1992).
[33] P. Manneville, *Dissipative Structures and Weak Turbulence* (Academic, New York, 1990).
[34] H. Sakagushi, Prog. Theor. Phys. **86**, 759 (1991); S. Sasa, *ibid*. **84**, 1009 (1990).
[35] V. Dufiet and J. Boissonade, J. Chem. Phys. **96**, 664 (1991).
[36] V. Dufiet and J. Boissonade, Physica A **188**, 158 (1992).
[37] J. Verdasca, A. De Wit, G. Dewel, and P. Borckmans, Phys. Lett. A **168**, 194 (1992).
[38] L. M. Pismen, in *Dynamics of Nonlinear Systems*, edited by V. Hlavacec (Gordon and Breach, New York, 1986), p. 47.
[39] F. H. Busse, J. Fluid Mech. **30**, 625 (1967).
[40] S. Ciliberto, P. Coullet, J. Lega, E. Pampaloni, and C. Perez-Garcia, Phys. Rev. Lett. **65**, 2370 (1990).
[41] In Rayleigh-Bénard convection, this quadratic term is related to the non-Boussinesq effects and normally appears as a small correction.
[42] I. Lengyel and I. R. Epstein, Science **251**, 650 (1991); I. Lengyel, S. Kadar, and I. R. Epstein, *ibid*. **259**, 493 (1993); I. Lengyel and I. R. Epstein, in *Chemical Patterns and Waves* (Ref. [7]), p. 297.
[43] This technical trick could be avoided by using a borned spatial profile such as a Gaussian, but the number of free parameters would increase.